Gaining Insights into the Function of Post-Translational Protein Modification Using Genome Engineering and Molecular Cell Biology

Meret Schmidhauser [1,†], Peter F. Renz [1,2,†], Panagiota Tsikrika [1,2,†], Remo Freimann [1], Anton Wutz [1], Jeffrey L. Wrana [3] and Tobias A. Beyer [1]

*1 - **Institute for Molecular Health Sciences,** ETH Zurich, Switzerland*
*2 - **Life Science Zurich Graduate School,** Molecular Life Science program, University of Zürich, Switzerland*
*3 - **Lunenfeld-Tanenbaum Research Institute,** Toronto, Ontario, Canada*

***Correspondence to Tobias A. Beyer:** IMHS, ETH Zurich, HPL J16, Otto-Stern-Weg 7, 8093 Zurich, Switzerland. tobias.beyer@alumni.ethz.ch*
https://doi.org/10.1016/j.jmb.2019.07.015

Abstract

Modifications by kinases are a fast and reversible mechanism to diversify the function of the targeted proteins. The OCT4 transcription factor is essential for preimplantation development and pluripotency of embryonic stem cells (ESC), and its activity is tightly regulated by post-transcriptional modifications. Several phosphorylation sites have been identified by systemic approaches and their functions proposed. Here, we combined molecular and cellular biology with CRISPR/Cas9-mediated genome engineering to pinpoint the function of serine 12 of OCT4 in ESCs. Using chemical inhibitors and an antibody specific to OCT4 phosphorylated on S12, we identified cyclin-dependent kinase (CDK) 7 as upstream kinase. Surprisingly, generation of isogenic mESCs that endogenously ablate S12 revealed no effects on pluripotency and self-renewal, potentially due to compensation by other phosphorylation events. Our approach reveals that modification of distinct amino acids by precise genome engineering can help to clarify the functions of post-translational modifications on proteins encoded by essential gene in an endogenous context.

Introduction

Modification of proteins by post-translational modifications (PTM), in particular phosphorylation by kinases, has been recognized as a powerful mechanism to diversify reversibly the functions of proteins. Over the last decades, countless phosphorylation sites have been identified on virtually every protein by mass spectrometry approaches. However, for the majority of the identified sites, the responsible kinase and the biological function remain unknown [1,2]. Inhibition or genetic ablation of kinases often leads to profound perturbation of the targeted cells or tissues, making it difficult to pinpoint causal phosphorylation events on the target proteins (e.g., Ref. [3]). Traditionally, scientists used genetic ablation of the target protein followed by complementation assays using cDNA coding for the deleted protein containing mutation(s) for the sites of interest [4]. This approach, though, is hampered when the protein of interest is essential for the cell.

OCT4 (aka OCT3 or POU5F1) is encoded by the *POU5F1* gene, belongs to the family of the octamer-binding group of POU transcription factors (TFs) [5] and is expressed in oocytes, embryonic carcinomas, germ cells and most importantly in embryonic stem cells (ESCs; reviewed in Ref. [6]). Together with SOX2 and NANOG, OCT4 is the dominating member of the core pluripotency TFs. This protein is responsible for maintaining the ESC state by activating genes crucial for pluripotency and repressing genes involved in lineage specification (reviewed in Refs. [7,8]). OCT4 can be therefore considered as an essential protein for the function of ESCs. OCT4 binds to DNA by a central bipartite motif composed of two helix-turn-helix domains (POU-specific/POU homeo-domain), and the transcriptional activity is provided by two proline-rich

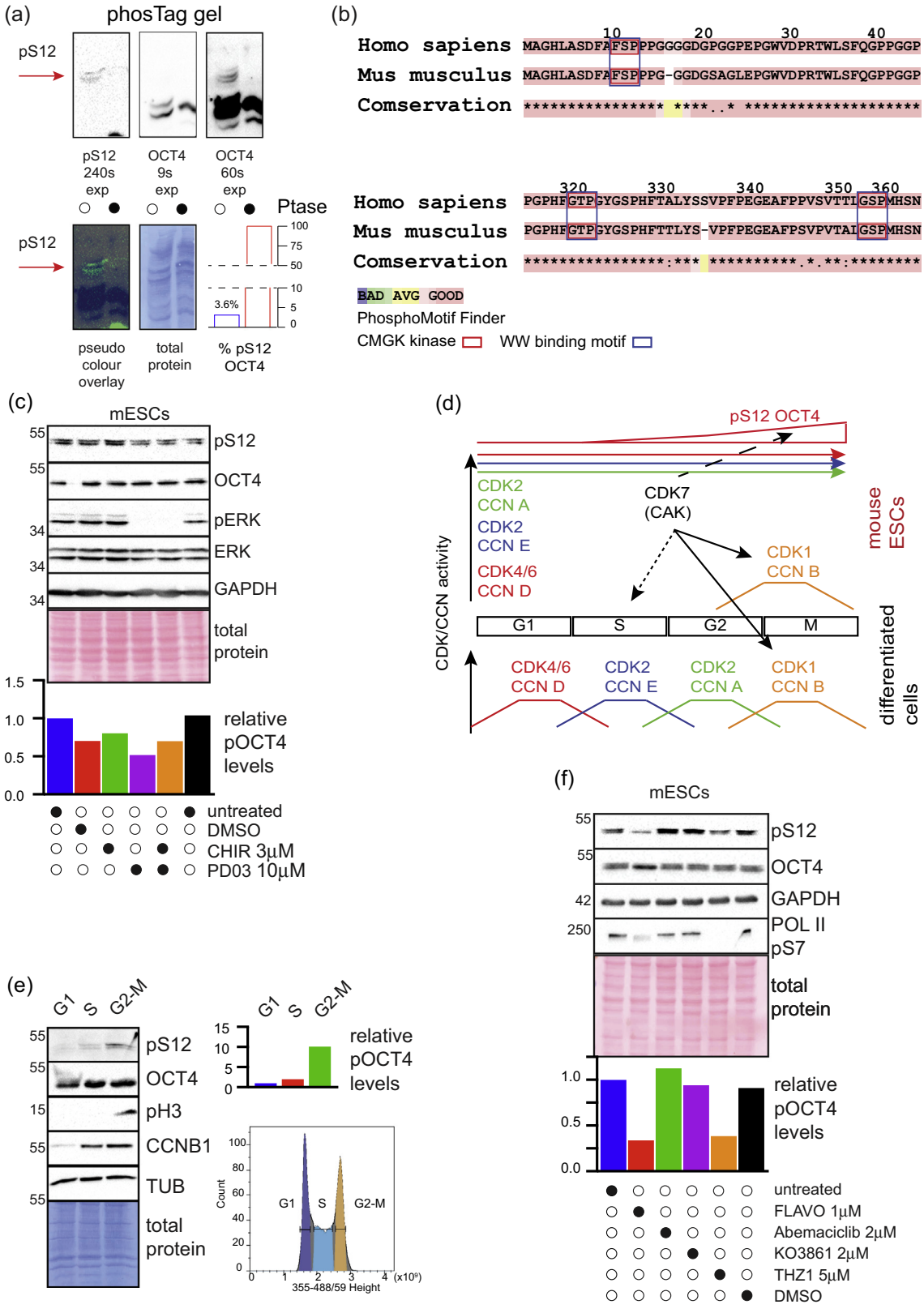

Fig. 1 (*legend on next page*)

domains (N- and the C-terminus) [9,10]. Importantly, OCT4 protein levels are controlled and fine-tuned by post-transcriptional and post-translational mechanisms. PTMs (e.g., ubiquitinylation or phosphorylation) have been shown to modulate subcellular localization, protein stability, transcriptional activity or protein–protein interactions [6,11,12]. According to PhosphoSitePlus, OCT4 has at least 19 (human and mouse) amino acids modified by protein kinases and only 4 (human) or 2 (mouse) have a molecular function attributed [13]. These modifications were mainly identified in high-throughput approaches such as mass spectrometry [14], by indirect *in vitro* assays [15], in cell lines overexpressing OCT4 or during reprogramming of somatic cells to induced pluripotent stem cells [12]. Recently, Liu *et al*. [3] identified CyclinE/CDK2 to be the kinase phosphorylating OCT4 on serine 12 (S12), serine 355 (S355) and threonine 322 (T322) by elegantly combining genetics and biochemistry. Knockout of all five G1 cyclins (D1, D2, D3, E1 and E2) in mESCs (coined Q-KO cells) and consequent inactivation of CDK2/4/6 leads to perturbation of the pluripotent state and to the adaption of the trophectoderm cell fate. This was attributed to reduced phosphorylation of OCT4 (as well as SOX2 and NANOG) leading to an increase of protein turnover [3]. Phosphorylation of OCT4 on S12 has been previously implicated to stabilize OCT4 by binding to PIN1, thereby preventing ubiquitinylation by WWP2 [12].

Here, we developed a workflow to address the function of a previously identified phosphorylation site at the endogenous level on an essential protein by combining molecular cell biology and genome engineering. Using small-molecule inhibitors and an antibody specific to OCT4 phosphorylated on S12, we identified CDK7 as the upstream kinase. Surprisingly, ablation of S12 in mESCs by CRISPR/Cas9-mediated genome engineering revealed no apparent phenotype in pluripotency and self-renewal contrasting the findings obtained by high-throughput studies or genetic ablation of all G1-CDK activity [3]. A possible explanation for the lack of phenotype in the generated cell lines is a compensation mechanism by redundant sites (e.g., T322 and S355).

Thus, we propose to use our workflow presented here, to systematically characterize phosphorylation sites that have been proposed to have essential functions, to gain a deeper understanding in their role in biological processes.

Results and Discussion

OCT4 is phosphorylated on serine 12 in ESCs

Phosphorylation of OCT4 by kinases provides a potential mechanism to regulate OCT4 activity through signaling molecules. Several phosphorylation sites have been identified [12,14–16], and recent work found that CyclinE/CDK2 can phosphorylate OCT4 on serine 12 (S12), serine 355 (S355) and threonine 322 (T322) *in vitro* [3].

Given the fact that S12 is highly conserved in mammals, lies within the N-terminal transactivation domain and has been shown to mediate protein–protein interactions [12], we decided to focus on S12 and to investigate the function of phosphorylated S12 in an endogenous context. We first generated an antibody specific for OCT4 phosphorylated at S12 and characterized its specificity. siRNA-mediated knockdown of OCT4 in human embryonic stem cells (hESCs) revealed that the antibody recognizes OCT4 protein (Fig. S1a). Treating immunoprecipitated total OCT4 protein from H9 hESCs with alkaline phosphatase indicated that the antibody recognizes only phosphorylated OCT4 (Fig. S1b). To show that the antibody only binds to OCT4 phosphorylated on S12, we expressed wild type (wt) hOCT4 or hOCT4 carrying a 12S-A substitution ectopically in HEK293T cells. The antibody only recognized the phosphorylated wt protein but not the 12S-A mutant (Fig. S1c). Given the fact that the peptide used for immunization is 100% conserved between human and mouse OCT4, we assumed that

Fig. 1. OCT4 pS12 phosphorylation is downstream of CDK7. (a) PhosTag SDS-PAGE electrophoresis of lysates from wt cells. OCT4 (exposure of 9 and 60s) and pS12 OCT4 were detected by immunoblot on the same membrane and the signal overlayered in pseudo-colors. Quantification of pS12 OCT4 levels was calculated and depicted as % of total OCT4 levels. Cell lysates treated with phosphatase served as negative controls. (b) Sequence alignment of human and mouse OCT4 protein fragments containing potential CMGK phosphorylation sites. (c) Immunoblot analysis of pS12 OCT4 after treating mouse ESCs with GSK3β (CHIR), MEK (PD03) inhibitor or both for 2 h. Phosphorylation of ERK1/2 is abolished after treatment with inhibitors targeting MEK. Relative pS12 OCT4 levels are visualized as bar graphs. (d) Cartoon illustrating the regulation of CDKs during the cell cycle in ES and differentiated cells. Direct and indirect targets of CDK7 are indicated. (e) Immunoblot showing the distribution of pS12 OCT4 during the cell cycle. Relative pS12 OCT4 levels are visualized as bar graphs. Phosphorylated H3 and CCNB1 are used to show the purity of the cells enriched by FACS. Histogram of the cells sorted according to their DNA content. (f) Immunoblot analysis of pS12 OCT4 and OCT4 in mESCs after treatment for 2 h with CDK inhibitors as indicated. Relative pS12 OCT4 levels are visualized as bar graphs. Phosphorylation of POL II S7 is diminished after treatment with inhibitors targeting atypical CDKs. Staining of immunoblot membranes with anti GAPDH/TUBULIN antibodies and staining of the membrane with Ponceau or Coomassie ensured equal loading. All experiments were performed at least three times ($N \geq 3$), and representative images are shown.

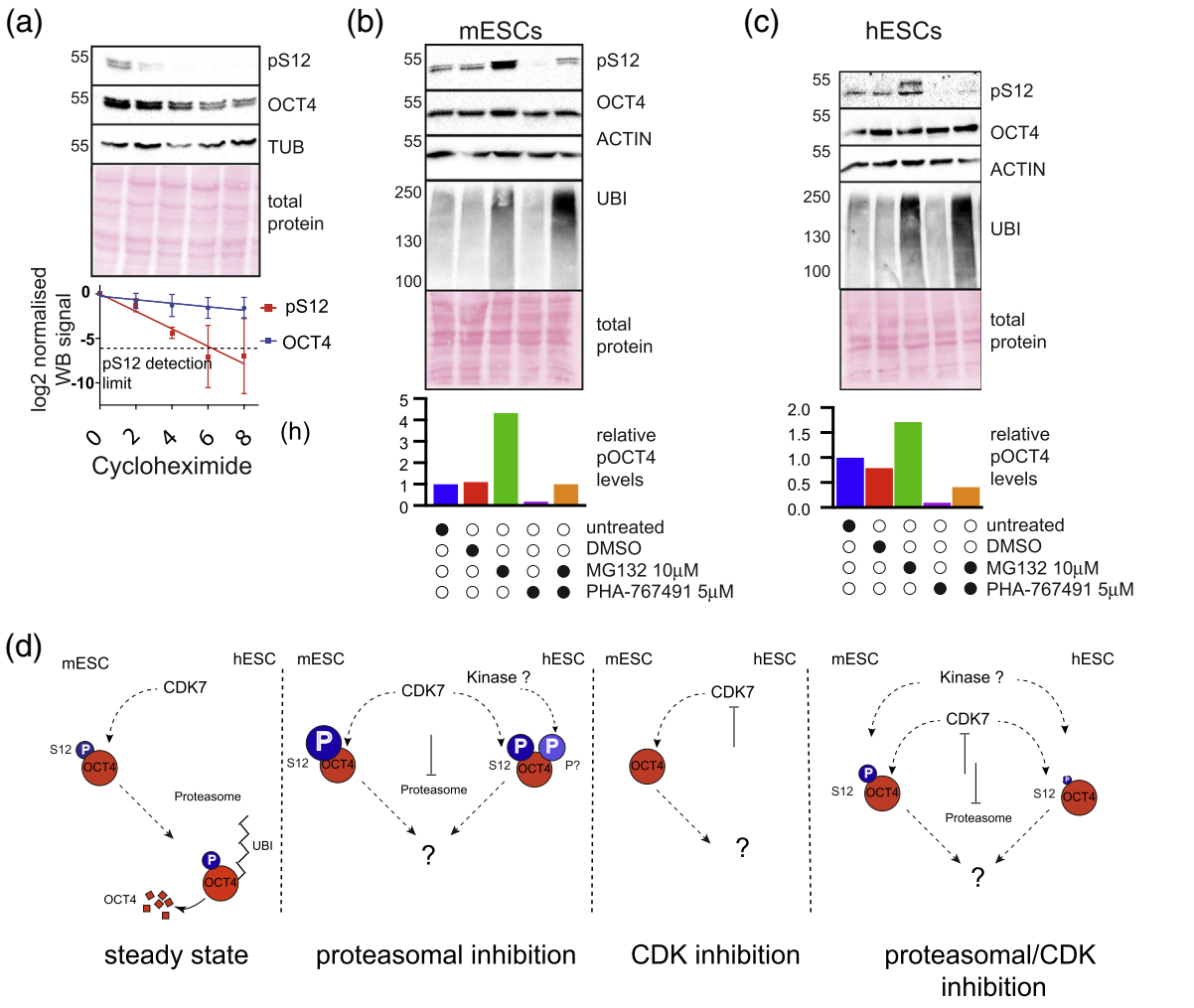

Fig. 2. Phosphorylation of S12 is targeting OCT4 for proteasomal degradation. (a) Cycloheximide chase experiment showing the protein turnover rates of pS12 OCT4 and OCT4. The detection limit of the pS12 OCT4 antibody is indicated by a dashed line. (b + c) pS12 OCT4 is targeted to the proteasome in mouse (b) and human (c) ESC. Relative pS12 OCT4 levels are show as bar graphs. Accumulation of ubiquitinylated proteins indicates the effectiveness of the 2-h proteasomal inhibition. Staining of immunoblot membranes with anti GAPDH/TUBULIN antibodies and staining of the membrane with Ponceau or Coomassie ensured equal loading. All experiments were performed at least three times (N ≥ 3), and representative images are shown. (d) Cartoon summarizing the results from panel (b + c).

the antibody will recognize murine pSer12 OCT4 efficiently.

Phosphorylation on a specific site occurs often at a sub-stoichiometric ratio depending on the cell type and state [1]. To evaluate the extend of OCT4 phosphorylation on S12 in mouse (m)ESCs, we performed PhosTag gel electrophoresis, a method that allows to more efficiently separate phosphoproteins (Fig. 1a) [17] and noted that OCT4 is indeed highly phosphorylated as we observed four distinct OCT4 phosphoproteins suggesting multiple modifications. Interestingly, overlaying the signals from the total OCT4 and the pS12 OCT4 immunoblot and quantifying it, revealed that only a small portion (3.6%) of OCT4 is phosphorylated at S12. In addition, we observed that pS12 is present at two distinct bands, suggesting that this site acts in concert with other phosphorylation events.

CDKs phosphorylate OCT4 on S12

In order to identify all potential kinases phosphorylating OCT4 S12, we used PhosphoMotif Finder [18]. Although prediction of kinase/substrate interactions based on short sequence motifs is unreliable [19], S12 was identified by PhosphoMotif Finder as a target of the CMGC [cyclin-dependent kinases (*C*DKs), mitogen-activated protein kinases (*M*AP kinases), glycogen synthase kinases (*G*SK) and *C*DK-like kinases families] group of kinases (Fig. 1b). This observation is in line with the report that CyclinE/CDK2 can phosphorylate OCT4 on S12

[3]. In order to understand the function of this phosphorylation and to integrate it into a cellular context, we aimed to identify the responsible CDK and potential additional kinases phosphorylating OCT4 on S12.

MAP and GS kinases play essential roles in the establishment of naïve pluripotency in mESCs [20]. These kinases might mediate their functions in mESCs by phosphorylating OCT4. To test this hypothesis, we used small-molecule inhibitors to block the activity of MEK and GSK3β in mouse and human ESCs. After inhibiting MEK, GSK3β or both kinases simultaneously, we observed a strong decrease in phosphorylated ERK1/2, but no obvious differences in phosphorylation of OCT4 S12 compared to untreated or DMSO-treated cells as illustrated in the quantification of the blots (Fig. 1c + S1d).

Next, we inhibited CDKs with flavopiridol (inhibition of CDK1/2/4/6/7, IC50 are listed in Table S1) in ESCs and observed a dramatic reduction of pS12 in both mESCs and hESCs (Fig. S1e) compared to untreated or DMSO-treated cells as illustrated in the quantification of the blots. Typical CDKs (e.g., CDK1–6) play crucial roles in the cell cycle, and atypical CDKs (e.g., CDK7–9) have functions in transcriptional regulation acting by phosphorylating the tail of the RNA polymerase II [21]. In addition, CDK7, together with CYCLIN (CCN) H, can act as cyclin-activating kinase (CAG) to regulate the activity of CDK2 and CDK1/CCN complexes in G1 or in G2 phases of the cell cycle, respectively [22]. In contrast to differentiated cells, murine and, to some extent, human ESCs exhibit a distinct regulation of the cell cycle; for example, they have constitutive active CDK2/4/6 and CCNA/E/D complexes and only CDK1/CCNB is activated in G2/M phase [23,24] (illustrated in Fig. 1d). To explore a potential link between cell cycle progression, CDK activity and pS12 OCT4, we performed fluorescence activated cell sorting (FACS) on mESCs according to their DNA content to enrich for the different cell cycle phases (G1, S, G2-M). Immunoblot analysis revealed a strong enrichment of pS12 OCT4 in the G2-M phase compared to the G1 and, to lesser extent, to the S phase of the cell cycle as illustrated by quantifying the relative amounts of pS12 OCT4 (Fig. 1e). These findings suggest a link to cell cycle progression. The purity of the fraction was confirmed by immunoblot with antibodies against phospho histone 3 and CCNB1 (Fig. 1e). To further narrow down the responsible kinase, we used small-molecule inhibitors targeting subsets of CDKs with different IC50: SNS-032 (CDK2/7/9), PHA-767491 (CDC7/CDK1/2/9) and NSC693868 (CDK1/5) (Table S1). We found that SNS-032 and PHA-767491, but not NSC693868 reduced pS12 OCT4 levels in mESCs (Fig. S1e, left panel), with similar results in hESCs (Fig. S1e, right panel) compared to untreated or DMSO-treated cells. Monitoring total OCT4, we found that SNS-032 and PHA767491 did not affect total OCT4 protein level, but instead changed the band migration pattern correlating with changes in phosphorylation of OCT4. These results suggest that CDK2, CDK7 or CDK9 might act as upstream kinase for S12.

To further narrow down the responsible CDK, we treated mESCs with next-generation CDK inhibitors with increased specificity [Abemaciclib (CDK4/6), K03861 (CDK2) and THZ1 (CDK7)]. Immunoblot analysis revealed that only THZ1, a covalent CDK7 inhibitor, reduced pS12 OCT4 levels, although to a lesser extent than flavopiridol (Fig. 1f), whereas inhibition of CDK2/4/6 had no effect compared to untreated or DMSO-treated cells.

In summary, these findings show that OCT4 is phosphorylated on S12 mainly by CDK7. In addition, we could show that this modification accumulates in the G2/M phase of the cell cycle in mESCs. This partially confirms previous results linking this PTM to cell cycle progression [3], but suggests a more complex mechanism of regulation (Fig. 1d).

P-Serine 12 regulates OCT4 protein stability

WWP2 is a HECT E3 ubiquitin ligase with four WW domains. These domains serve as substrate recognition modules and bind with high affinity to PPxY or pS/T-P motifs [25]. OCT4 is bound and polyubiquitinylated by WWP2, which leads to degradation by the proteasome [26]. Degradation of OCT4 was hypothesized to be blocked by PIN1 through binding via its WW domain to pS12 [12]. In mESCs lacking all five G1 cyclins (D1, D2, D3, E1 and E2, coined Q-KO cells), OCT4 no longer binds to PIN1 and has an increased protein turnover rate [3]. The authors, however, did not test directly whether this is associated with OCT4 phosphorylation on S12, but only assessed the extent of all S/T-P phosphorylation. Furthermore, these Q-KO mESCs spontaneously differentiate into trophectoderm cells, thereby losing pluripotency and expression of pluripotency factors.

To test whether pS12 is indeed involved in OCT4 protein stability, we took advantage of our pS12 OCT4 antibody and performed cycloheximide-chase experiments with mESCs. The half-life of total OCT4 was calculated by linear regression of log2 normalized immunoblot signal to be approximately 3.5 h, whereas the half-life of OCT4 phosphorylated on S12 was around 1 h (Fig. 2a). However, the pS12 OCT4 signal is weak and not reliably detectable beyond 4 h of cycloheximide treatments (indicated by a dashed line in Fig. 2a). Nevertheless, this indicates that either OCT4 phosphorylated on S12 is less stable than the unmodified protein, or alternatively, the activity of the corresponding phosphatase is altered.

In order to confirm these observations, we treated mESCs for 2 h with MG132, a proteasomal inhibitor, and observed a stabilization of the pS12 OCT4 compared to untreated or solvent treated control cells

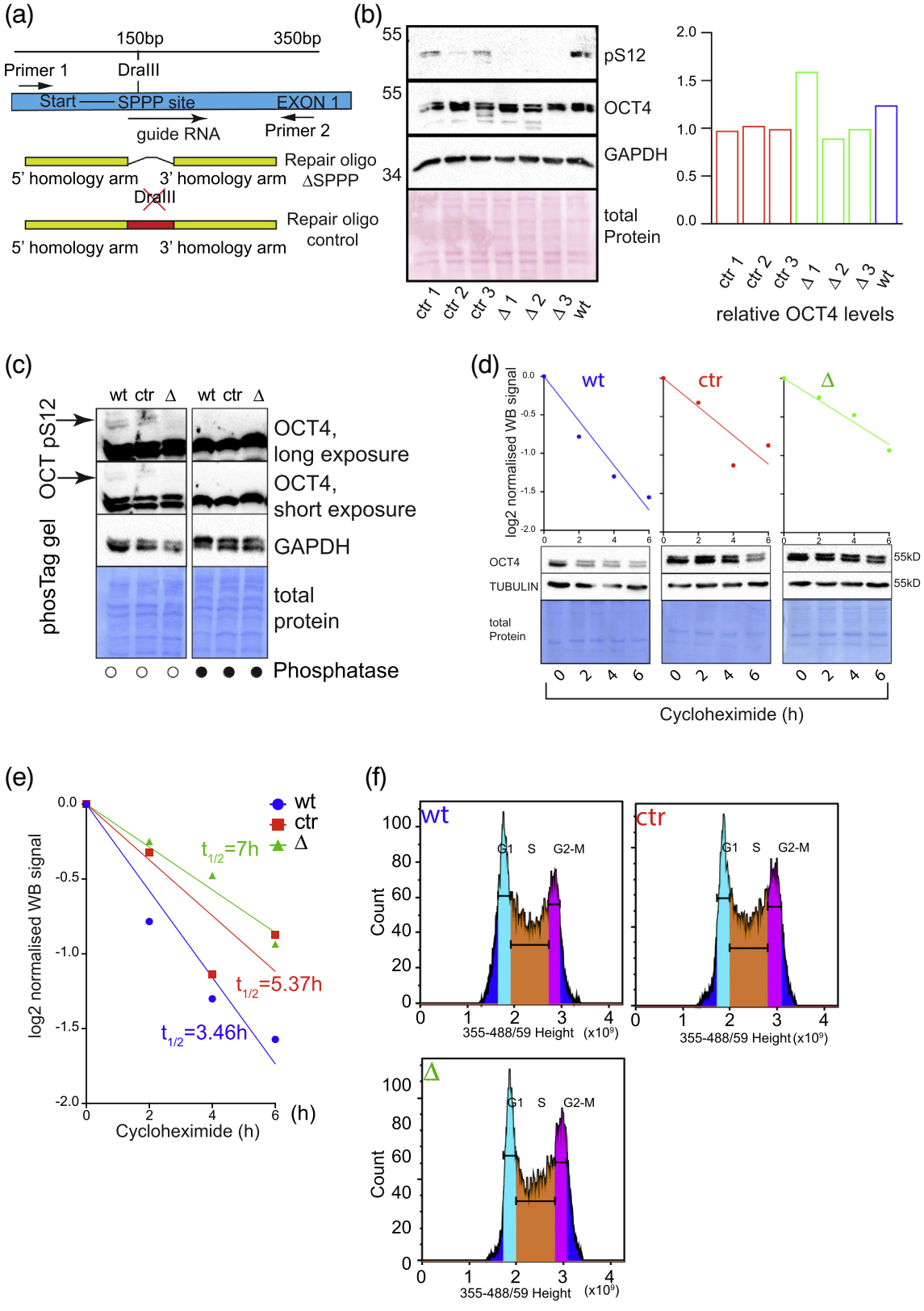

Fig. 3 (*legend on next page*)

(Fig. 2b, mouse; Fig. 2c, human). We did not observe stabilization of total OCT4 and ACTIN levels confirming our previous result (Fig. 2a) that OCT4 phosphorylated on S12 is more rapidly turned over by the proteasome. Interestingly, quantification of the immunoblot signals revealed that the overall effect of proteasome inhibition on pS12 levels was more pronounced in mESCs compared to hESCs. Furthermore, we observed an additional phosphorylation on OCT4 in hESCs upon proteasomal inhibition. Overall, these results show clearly that OCT4 phosphorylated on S12 is targeted by the proteasome. Surprisingly, combining CDC7/CDK1/2/9 inhibition with MG132 leads to phosphorylation levels of OCT4 on S12 comparable to control cells in mESCs (Fig. 2b) and to intermediate levels in hESCs (Fig. 2c). In summary, these experiments suggest that turnover of pS12 OCT4 is controlled by a complex mechanism that might involve additional kinase(s) and is divergent in human and mouse ESCs (Fig. 2d) and therefore begs further investigation in the future.

Our results are in contradiction with previous reports [3,12]. This discrepancy most likely arises due to the fact that in Q-KO mESCs, OCT4 phosphorylation is not only abolished on S12, but also T322 and S355. Both amino acids also form binding sites for WW domains upon phosphorylation and might act in concert with S12 (Fig. 1b). Overall, this suggests a complex mechanism of action, and we decided to generate pS12 OCT4 mutant mESC lines to investigate the function of this modification.

Generation of OCT4 Ser12 mutant mESC lines

In order to address the discrepancies between ours and the previously published results [3,12] and to dissect the functions of pS12 OCT4 in an endogenous context, we decided to create mESCs harboring a mutation of the CDK7 target site on OCT4 using a CRISPR/Cas9 based knock-in approach by removing the entire SPPP motif (residues 12–15). The rationale behind this approach was (1) to remove not only the site of the PTM, but also the motif recognized by the kinase [27] and protein interaction partners that bind this motif via WW domains [28], and (2) to facilitate the screening for mutant *Oct4* clones by genomic PCR and restriction digests. The strategy to target the site in *Oct4* is summarized in Fig. 3a and described in detail in the Methods section. In brief, cells were transfected with a plasmid containing the guide RNA sequence/Cas9 protein and either a control or the knock-out repair template (Fig. S2a). Isolated clones were screened and mutated cells identified by PCR and restriction enzyme digests (Fig. S2b). Sequencing of the PCR product from genomic DNA of control (ctr) and delta SPPP (Δ) cells revealed that all control (ctr) clones retained at least one functional *Oct4* allele, whereas Δ clones had deletions of the SPPP motive on either both alleles or on one allele and a premature stop on the second allele (Fig. S2c). In order to obtain the cell lines used in this study, we were forced to screen more than 600 individual clones, most likely due to the fact that *Oct4* is an essential gene in mECSc.

We isolated total proteins from all sequenced clones and verified pS12 OCT4 levels by immunoblotting. All control lines (ctr.1–3) had detectable pS12, whereas the knock-in cells (Δ 1–3) showed no signal (Fig. 3b). This indicates that we generated loss of pS12 OCT4 as well as corresponding isogenic ctr cell lines.

Our previous experiments using phosTag gel electrophoresis indicated that OCT4 is phosphorylated on multiple residues, while only a small percentage is corresponding to pS12 (Fig. 1a). We speculated that pS12 might act in concert and is redundant with similar sites within the OCT4 protein (Fig. 1b). In order to assess whether ablation of pS12 has an effect on the abundance of other OCT4 phospho forms, we performed phosTag gel electrophoresis [17]. Migration pattern of OCT4 in Δ cells compared to wt and ctr cells showed that only a small subset of the phosphorylation events on OCT4 correspond to pS12 confirming our initial result (Fig. 3c). In addition, we were not able to detect alteration in other phosphorylation events on OCT4 upon S12 deletion.

Overall, these results show that we generated mutant mESCs bearing an ablation of S12 on OCT4. Our study is, to our knowledge, the first to use CRISPR/Cas9 genome engineering to generate cell lines carrying a mutation on OCT4 to probe the functions of individual amino acids at the endogenous level.

pS12 depletion stabilizes OCT4 protein

Our previous results showed that pS12 OCT4 is more rapidly degraded by the proteasome compared to the unmodified protein (Fig. 2). Therefore, we performed cycloheximide-chase experiments to test

Fig. 3. Generation and characterization of OCT4 S12 mutant cells. (a) Cartoon illustrating the CRISPR/Cas9 knock-in strategy. (b Immunoblot analysis for pS12 OCT4 and total OCT4 proteins in wt, ctr and Δ cell lines. Relative total OCT4 protein levels were quantified and illustrated as bar graphs. (c) PhosTag SDS-PAGE electrophoresis of lysates from wt, ctr and Δ cells. OCT4 was detected by immunoblot, and two different exposures are shown. Cell lysates were treated with phosphatase served as negative controls. (d) Cycloheximide chase experiment showing differences of OCT4 protein turnover rates in wt (blue), ctr (red) and Δ (green) cells. Plots show mean (N = 3). Representative immunoblots are shown for each mutant line. OCT4 signals were normalized to TUBULIN and total protein (Coomassie). The 0-h time point was set as 1, and the relative expression of OCT4 signal during the time course calculated as log2 fold change. The protein half-life ($t_{1/2}$) was determined by linear regression. (e) Overlay of the linear regression of the wt, ctr and Δ cells. (f) Representative cell cycle histograms of wt (blue), ctr (red) and Δ (green) cells (N = 3).

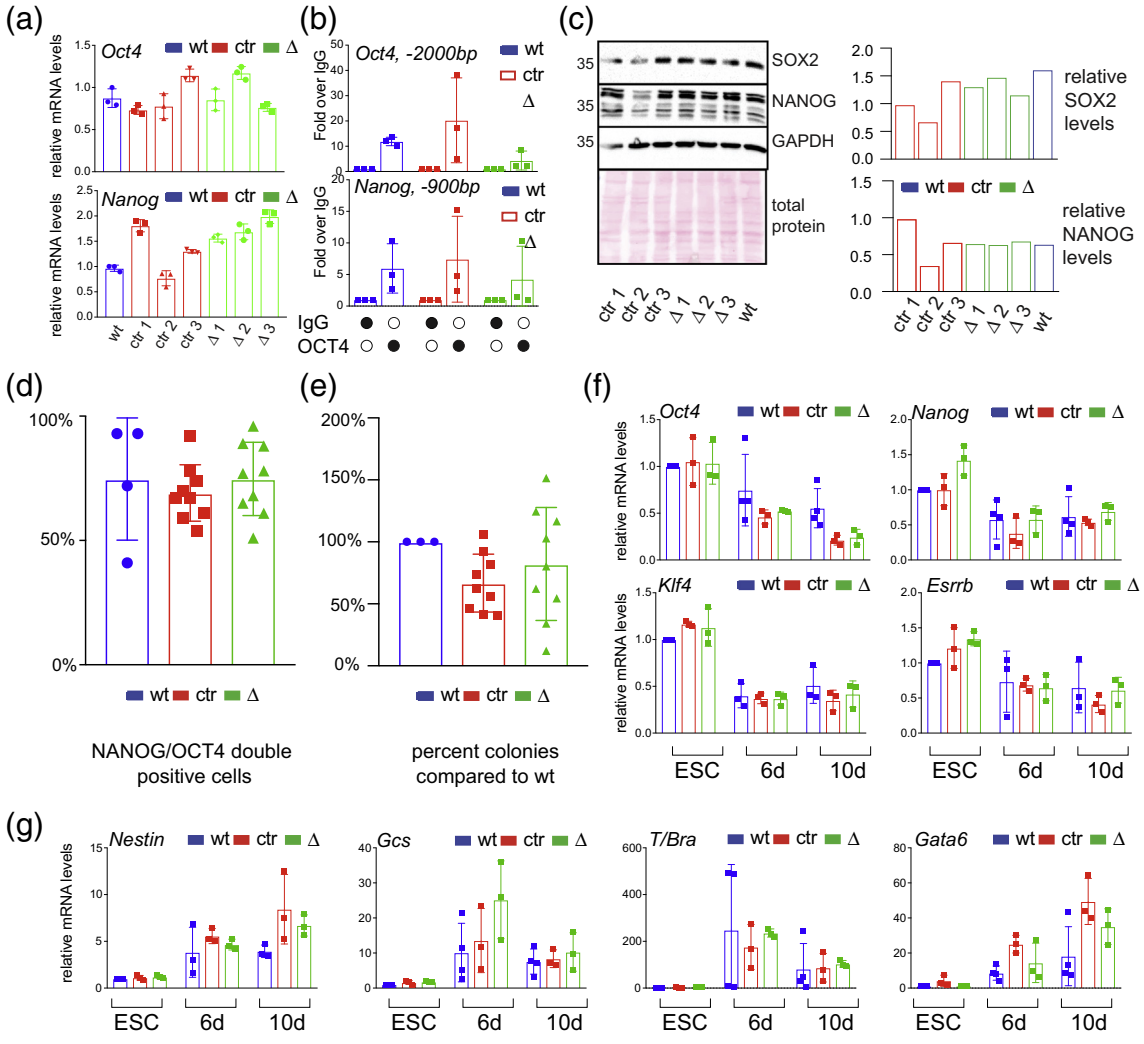

Fig. 4. Ablation of S12 has no impact on self-renewal and pluripotency in mESCs. (a) qRT-PCR measuring relative *Oct4* and *Nanog* mRNA expression levels in wt (blue) ctr (red) and Δ (green) cells. mRNA expression levels of tested genes were normalized to *Gapdh* and *Rrm2* using the ΔΔct method. Scatter plots show mean expression levels ± SD (N ≥ 3). Data points indicate the expression level of individual clones. (b) OCT4 binding to DNA regulatory elements on the *Oct4* and *Nanog* genomic loci was determined by ChIP-qPCR. Signal was normalized to input and calculated as fold enrichment over IgG control precipitations. Scatter plots show mean ± SD, and individual points represent the signal of the individual clones (N = 3) [wt (blue), ctr (red) and Δ (green)]. (c) Immunoblots analysis of SOX2 and NANOG in wt, ctr, and Δ cell lines. Relative SOX2 and NANOG protein levels were determined and depicted as bar graphs. GAPDH and Ponceau stain insured equal loading (N = 3). (d) Flow cytometry analysis of the percentage of OCT4 and NANOG double-positive cells in wt (blue), ctr (red) and Δ (green) cells. Bar graphs show the average percentage ± SD of OCT4/NANOG double-positive cells (N ≥ 8). Individual data points indicate the percentage of OCT4/NANOG double-positive cells of the clones of the indicated genotype. (e) Clonality assay of wt, ctr and Δ cells. mESCs were plated at low density as single cells and the emerging colonies stained for alkaline phosphatase. Bar graph shows the average percentage (± SD) of colonies relative to the wt control cells. Individual points represent the values for individual replicates of the clones (f + g) qRT-PCR of indicative transcripts for pluripotency and differentiation after EB formation of pS12 OCT4 mutant ESCs. mRNA expression levels of tested genes were normalized to *Gapdh* and *Rrm2* using the ΔΔct method. Expression levels of wt cells were arbitrarily set as one. Scatter plots show mean expression levels ± SD (N ≥ 3). Individual data points indicate the expression level of one clone of the indicated genotype (average expression of at least two technical replicates).

whether OCT4 protein stability was affected in the mutant cell lines. We calculated OCT4 protein half-life ($t_{1/2}$) using linear regression of log2 normalized immunoblot signals and observed protein half-life of $t_{1/2}$ = 3.46 h for wt, $t_{1/2}$ = 5.37 h for ctr and $t_{1/2}$ = 7.0 for Δ cells (Fig. 3d + e), suggesting that ablation of S12 might lead to a decrease in protein turnover. However, goodness-of-fit analysis in PRISM 8 indicated high variances (Sy.x for wt = 0.8267, ctr = 0.5875, Δ = 0.2542), making these results difficult to interpret.

Alteration of pS12 on OCT4 has no effect on cell cycle progression of mESCs

mESCs have an altered cell cycle compared to somatic cells [24] and have different propensities to differentiate towards the individual germ layers in function of the cell cycle state [23] (Fig. 1d). Recent reports suggested a non-transcriptional role of OCT4 in the regulation of mitotic entry controlling CDK1 activity by antagonising COPS2 [29,30]. As OCT4 pS12 is accumulated during the G2-M phase of the cell cycle (Fig. 1e), we speculated that modification of S12 might impact the regulation of CDK1 activity subsequently affecting the cell cycle of the mutant cells. Therefore, we performed cell cycle analysis and observed no significant differences between wt, ctr, and Δ cells (Fig. 3f).

Surprisingly, our results so far indicate a rather mild phenotype of the mutant cell lines with only minor effects on OCT4 protein turnover rates in Δ cells and no alteration in cell cycle progression.

Serine 12 phosphorylation is dispensable for self-renewal and pluripotency of mouse ES cells

The generation of the isogenic S12 OCT4 mESC lines involved extensive screening of more than 600 clones. We observed clonal effects on pS12 levels in some of the ctr cell lines; for example, ctr1 *versus* ctr2 (Fig. 3b). In addition, total OCT4 protein levels were also subject to minor fluctuations (Fig. 3b). We therefore decided to perform a thorough characterization of the generated cell lines and investigated, whether pS12 has an effect on the transcriptional activity of OCT4 in pluripotent cells. It has been shown previously that the N- and C-terminal glycine/proline-rich domains have transactivation properties, and deletion studies showed that they act redundantly [10]. Nevertheless, to show that deletion of the SPPP motif did not interfere with the ability of OCT4 to regulate transcription, we performed RT-qPCR with primers specific to *bonae fidae* target genes of OCT4 [29,30]. mRNA Expressions of *Oct4*, *Nanog*, *Sox2*, *Ffg4*, *Rex1* (*a.k.a Zfp42*) *and Dnmt3a* in ctr and Δ cells were similar compared to wt cells (Fig. 4a + S3a). However, we observed slight clonal variations without evident link to the genotype of the cells. Furthermore, expression levels of *Klf4* and *Esrrb*, two factors implicated in the pluripotent state [31], showed no apparent dysregulation in the mutant cells (Fig. S3b). In addition, we tested the DNA binding activity of OCT4 in wt, ctr and Δ cells by performing ChIP-qPCR experiments amplifying well-characterized OCT4 binding sites (*Oct4* and *Nanog* enhancer) [29,30] (Fig. 4b).

We concluded that phosphorylation on S12 has no direct effect on OCT4's capability to regulate transcription in the pluripotent state. Immunoblot analysis revealed, that SOX2 and NANOG levels were not altered in ctr, and Δ cells compared to wt cells (Fig. 4c). NANOG has been shown to have a dynamic, mosaic expression pattern in mESCs grown in serum/LIF conditions [32]. The expression of NANOG fluctuates between high and almost non-detectable levels and is present in about 70%–80% of OCT4-positive cells in serum/LIF conditions at a given time point. Cells expressing low levels of NANOG are more prone to differentiate, and the percentage of NANOG low-expressing mESCs in a culture can be used as proxy to investigate the "stemness" of mESC cultures [33]. We used FACS (Fig. 4d, gating strategy Fig. S3c) [34] and immunofluorescence (Fig. S3d) with NANOG and OCT4 antibodies to investigate potential disturbances of self-renewal in the mutants. The fraction of OCT4/NANOG double-positive cells were similar between all cell lines indicating a comparable degree self-renewal. To strenghten this observation, we addressed the ability of the generated cell lines to form colonies from single cells. For this, we seeded 3–4 cells/cm^2 and and stained the formed colonies for alkaline phosphatase [35]. Quantification revealed that ctr and Δ cells had similar colony-forming capacity compared to wt cells (Fig. 4e).

OCT4 protein levels are not only crucial for self-renewal but also initiation of cell fate specification and therefore pluripotency. We tested whether pS12 has an influence on cell fate specification and performed embryoid body formation (EB) (Fig. S3e). Interestingly, pS12 OCT4 levels were reduced drastically after 2 d of EB formation in wt cells and no longer detectable after 4 d of differentiation (Fig. S3g). In contrast, total OCT4 levels remained comparable to undifferentiated cell at day 2 and started to decline after 4 d of differentiation. Therefore, we speculated that pS12 might play a role in cell fate specification and performed EB differentiation assays with wt, ctr and Δ cells. Resolution of the pluripotent state and commitment to one of the embryonic germ layers (ectoderm, mesoderm and endoderm) were monitored by qRT-PCR of indicative transcripts. All cell lines were able to differentiate as they reduced the mRNA expression of *Oct4*, *Nanog*, *Klf4* and *Esrrb* with similar kinetics between wt, ctr and Δ cells (Fig. 4f). We did not observe evident differences in the expression of ectoderm markers (*Nestin*, Fig. 4g). Previous studies indicated a crucial role of OCT4 protein levels in specifying mesoderm and endoderm linages during gastrulation [36]. The primitive streak is the embryonic structure from which mesoderm and endoderm cells emerge after gastrulation [37]. We therefore tested whether ablation of S12 has an impact on differentiation of mESCs toward the primitive streak and subsequently mesoderm and endoderm. Monitoring the induction of the primitive streak marker *Gsc*, the mesoderm marker *T/Bra* and the endoderm marker *Gata6* during EB differentiation revealed no apparent defects in differentiation linked to the genotype of the mutant cells (Fig. 4g).

In order to confirm the results obtained by EB differentiation, we performed directed differentiation toward neurectoderm (Fig. S3h) [38], ExEn stem cells (XEN) (Fig. S3i) [39] and PS (Fig. S3j) [40]. RT-qPCR

with indicative transcripts confirmed our previous observation that wt, ctr and Δ cells have comparable differentiation capabilities.

In summary, our results identified the responsible kinase phosphorylating OCT4 on S12. Surprisingly, the genetic approach ablating S12 on OCT4 revealed no effect on self-renewal and pluripotency in mESCs.

Conclusions

Our study shows clearly the advantages, as well as the weaknesses in the current approaches to identify and functionally characterize PTM. Phosphoproteomics is a powerful approach to systematically identify all potential modifications on a distinct protein or to a certain extend in a cell type [1]. However, it provides only limited information on the functionality of the modification. On the other hand, genetic ablation of kinases can lead to complex phenotypes with multiple confounding causes as demonstrated by ablation of all CDK activity by inactivation of all five cell cycle cyclins [3]. Here, we chose a phosphorylation site on a TF that is essential for the cell type used, based on previously published data and dissected its function by molecular cell biology and CRISPR/Cas9-mediated genome engineering. We successfully identified the kinase acting upstream of pS12 OCT4. However, our approach yielded no apparent phenotype, suggesting that either the chosen site has no function or redundant sites were able to compensate. In the future, we will systematically characterize potential sites on OCT4 that might compensate for the loss of pS12 (e.g., T322 and S355) by the approach described in this report to gain a deeper understanding in their functions.

We present with this study a blueprint to pinpoint the functions of a previously identified phosphorylation site using systemic approaches into a cellular and organismal context. However, given the fact that the approach is tedious and time consuming, it will only be suitable to assess the functions of a small set of PTMs that have important functions implicated.

Experimental Procedures

Materials

Antibodies, primers, small-molecule inhibitors, cell culture medium composition and reagents are listed in Table S1.

Methods

OCT4 sequence analysis

OCT4 sequences from the species indicated were obtained from the NCBI database and aligned to the human protein using TCOFFE (http://www.ebi.ac.uk/Tools/msa/tcoffee/). Phospho-sites were identified with PhosphoMotif Finder (http://www.hprd.org/PhosphoMotif_finder) and annotated with PhosphoSitePlus (https://www.phosphosite.org//proteinAction?id=23945&showAllSites=true).

Differentiation of mESCs

Embryoid body differentiation was performed as described [39]. Cells (4×10^4) were seeded in one well of a spherical plate (https://www.kugelmeiers.com/) and cultivated in suspension in mESC medium without LIF for 6 days. Half of the spheres were harvested after 6 days in culture. The remaining cells were plated on gelatine-coated plates, left to adhere and harvested after a total of 10 days of differentiation. The medium was replenished every second day.

FACS analysis

Cells were trypsinized, collected by centrifugation, washed with PBS and fixed for 10 min at 37 °C with 4% formaldehyde solution (FA)/1× PBS. After fixation, the cells were washed with 1× PBS, permeabilized with ice-cold methanol/water (90%/10%) and washed again with PBS. Primary antibodies (ms α-OCT4 and rb α-NANOG) were applied to the cells for 1 h followed by PBS wash and incubation with corresponding fluorescent labeled secondary antibodies (Jackson Immuno Labs). Stained cells were analyzed by flow cytometry using a MoFloAsterios and double-positive cells counted as described previously [34]. Unstained cells and single-labeled cells served as controls to adjust for background and to compensation for double labeling. For the gating strategy, see Fig. S3c.

Cell cycle analysis by FACS

Cells were trypsinized, washed in 1× PBS and incubated with Hoechst fluorescent dye. The cells were analyzed on a MoFlo Asterios cell sorter. Cell cycle profiles were generated and quantified with Kaluza. For subsequent immunoblot analysis, 5×10^7 cells were resuspended in 1× PBS containing protease, phosphatase inhibitors and Hoechst. Cells were collected according to their DNA content using a MoFlo Asterios (G1, S and G2/M, at least 3×10^6 per cell cycle phase) and lysed in TNTE buffer (see below).

Immunofluorescence

mESCs (2×10^4) were plated on laminin coated roboz slides and grown for 24 h, fixed for 10 min in 4% FA/PBS. Fixed cells on roboz slides were washed with PBS, permeabilized and epitope blocked by incubation in 2% BSA/0.1% TritonX/1× PBS for 1 h. Primary antibodies were applied in blocking solution and incubated at 4 °C overnight.

Cells were subsequently washed with 1× PBS and incubated with the corresponding fluorescently labeled secondary antibodies. The slides were mounted in Mowiol containing DAPI. Z-stack images were acquired using identical settings for all corresponding conditions on a Zeiss Axio Observer and background fluorescence subtracted by deconvolution.

Immunoprecipitation and immunoblot

Cells were lysed in TNTE buffer [50 mM Tris/HCl (pH 7.6), 150 mM NaCl, 0.5% TritonX-100, 1 mM EDTA] containing protease and phosphatase inhibitors. Total OCT4 was precipitated using 1 μg of anti OCT4 antibody (BD) for 2 h at 4 °C, followed by incubation with 50 μl of 25%(V/V) Protein G slurry (Amersham) for 1 h at 4 °C. Precipitates were washed 5× with 1 ml 50 mM Tris/HCl (pH 7.6), 150 mM NaCl, 0.1% TritonX-100 and 1 mM EDTA; resuspended in 100 μl of TNTE containing no phosphatase inhibitors; and split in two. The precipitates were incubated for 30 min at 37 °C either with or without alkaline phosphatase (Fermentas). For immunoblot analysis, the beads were boiled with 2× Laemmli buffer and subjected to SDS-Page.

For immunoblot analysis, cells were lysed as described above and the protein content was determined by BCA protein determination kit (Pierce). Proteins were separated by SDS-PAGE, transferred to a nitrocellulose membrane and blocked in 5% non-fat dry milk in TBS-T [10 mM Tris/HCl (pH 7.5), 150 mM NaCl, 0.1% Tween 20]. The antibodies were applied in the blocking solution at the indicated dilutions (Table S1) at 4 °C overnight. The blots were washed three times with TBS-T, incubated with HRP coupled antibodies (Jackson Immuno Labs) and developed on a Bio-Rad imager using ECL (Pierce). Before re-exposing, the blots were incubated with stripping buffer [1 M glycine (pH 2.5), 0.5% SDS] for 1 h and extensively washed.

Quantification of immunoblots

Tiff images were exported at a resolution of 600 dpi from the Bio-Rad imager and loaded into ImageJ. The lanes marked and plotted and the area under the curve measured. The signal was normalized to the loading controls.

Cycloheximide chase experiment

mESCs were seeded at a density of 5×10^5 per 6 wells and grown in mESC medium. On the day of the experiment, the medium was replaced with fresh mESC medium containing 100 μg/ml cycloheximide and incubated for the times indicated. DMSO-treated cells served as control. Cells were lysed with TNTE and immunoblots performed as described above. The images of the blots were quantified using Fiji ImageJ. Signals were normalized to TUBULIN and total protein concentration visualized by Coomassie staining. OCT4 or pS12 OCT4 expression was normalized to total protein concentration and 0 h was set arbitrarily as 1. The relative expression of OCT4 in the time course was calculated, log transformed and plotted.

Statistical analysis

Linear regression and protein half-life was performed using PRISM 8.

RNA isolation and RT-qPCR

Total RNA was isolated using TRIzol according to the manufacturer's instructions. Total RNA (1 μg) was reverse transcribed using the Promega GoScript reverse transcription set and random hexamer primers. Quantitative real-time RT-PCR was performed with gene-specific primers (Table S1) and 2xSYBR green master mix (Kappa) using a Roche 480 light cycler. Relative expression levels of genes of interest compared to GAPDH and RRM2 were calculated using the ΔΔct method.

PhosTag gel electrophoresis

PhosTag gels were prepared according to the manufacturer instructions (Wako). Total proteins were isolated in TNT buffer (no EDTA) containing phosphatase and proteinase inhibitors. Proteins were separated by SDS-PAGE using an 8% acrylamide gel containing 50 μM PhosTag and 100 μM $MnCl_2$. In parallel, protein lysates were prepared as above, with the exception that no phosphatase inhibitors were added. Equal amounts of protein lysates were treated with phosphatase to serve as control.

Ethical statement

Experiments with hESCs were approved by the local and federal authorities (R-FP-S-1-0008-0000).

Supplementary data to this article can be found online at https://doi.org/10.1016/j.jmb.2019.07.015.

Acknowledgments

We thank Drs. C. Ciaudo and J.E. Corn for discussion and comments on the manuscript. This research was supported by ETH (Eidgenossische Technische Hochschule, Zurich, Switzerland) core

funding to the A.W laboratory and by LTRI (Lunenfeld-Tanenbaum Research Institute, Toronto, Ontario, Canada) core funding to the J.L.W. laboratory.

Author Contributions: M.S., P.F.R. and P.T. performed experiments. R.F. performed FACS analysis. A.W. and J.F.W. provided advice and corrected the manuscript. T.A.B. conceived, designed, performed, analyzed experiments and wrote the manuscript.

Conflict of Interest: The authors declare no conflict of interest.

Received 29 April 2019;
Received in revised form 3 July 2019;
Accepted 5 July 2019
Available online 12 July 2019

Keywords:
OCT4;
phosphorylation;
CDK;
CRISPR/Cas9;
mouse and human embryonic stem cells

Co-first author.

Abbreviations used:
ESC, embryonic stem cell; CDK, cyclin-dependent kinase; OCT4, octamer binding transcription factor 4; PTM, post-translational modification; CCN, cyclin; CAG, cyclin-activating kinase.

References

[1] E.J. Needham, B.L. Parker, T. Burykin, D.E. James, S.J. Humphrey, Illuminating the dark phosphoproteome, Sci. Signal. 12 (2019).
[2] M.G. Su, J.T. Weng, J.B. Hsu, K.Y. Huang, Y.H. Chi, T.Y. Lee, Investigation and identification of functional post-translational modification sites associated with drug binding and protein-protein interactions, BMC Syst. Biol. 11 (2017) 132.
[3] L. Liu, W. Michowski, H. Inuzuka, K. Shimizu, N.T. Nihira, J. M. Chick, et al., G1 cyclins link proliferation, pluripotency and differentiation of embryonic stem cells, Nat. Cell Biol. 19 (2017) 177–188.
[4] D. Cirera-Salinas, J. Yu, M. Bodak, R.P. Ngondo, K.M. Herbert, C. Ciaudo, Noncanonical function of DGCR8 controls mESC exit from pluripotency, J. Cell Biol. 216 (2017) 355–366.
[5] K. Okamoto, H. Okazawa, A. Okuda, M. Sakai, M. Muramatsu, H. Hamada, A novel octamer binding transcription factor is differentially expressed in mouse embryonic cells, Cell. 60 (1990) 461–472.
[6] S. Jerabek, F. Merino, H.R. Scholer, V. Cojocaru, OCT4: dynamic DNA binding pioneers stem cell pluripotency, Biochim. Biophys. Acta 1839 (2014) 138–154.
[7] J. Rossant, Genetic control of early cell lineages in the mammalian embryo, Annu. Rev. Genet. 52 (2018) 185–201.
[8] K.M. Loh, B. Lim, L.T. Ang, Ex uno plures: molecular designs for embryonic pluripotency, Physiol. Rev. 95 (2015) 245–295.
[9] M. Imagawa, A. Miyamoto, M. Shirakawa, H. Hamada, M. Muramatsu, Stringent integrity requirements for both trans-activation and DNA-binding in a trans-activator, Oct3, Nucleic Acids Res. 19 (1991) 4503–4508.
[10] H. Niwa, S. Masui, I. Chambers, A.G. Smith, Ji Miyazaki, Phenotypic complementation establishes requirements for specific POU domain and generic transactivation function of Oct-3/4 in embryonic stem cells, Mol. Cell. Biol. 22 (2002) 1526–1536.
[11] J.P. Saxe, A. Tomilin, H.R. Scholer, K. Plath, J. Huang, Post-translational regulation of Oct4 transcriptional activity, PLoS One 4 (2009), e4467.
[12] M. Nishi, H. Akutsu, S. Masui, A. Kondo, Y. Nagashima, H. Kimura, et al., A distinct role for Pin1 in the induction and maintenance of pluripotency, J. Biol. Chem. 286 (2011) 11593–11603.
[13] P.V. Hornbeck, B. Zhang, B. Murray, J.M. Kornhauser, V. Latham, E. Skrzypek, PhosphoSitePlus, 2014: mutations, PTMs and recalibrations, Nucleic Acids Res. 43 (2015) D512–D520.
[14] J. Brumbaugh, Z. Hou, J.D. Russell, S.E. Howden, P. Yu, A. R. Ledvina, et al., Phosphorylation regulates human OCT4, Proc. Natl. Acad. Sci. U. S. A. 109 (2012) 7162–7168.
[15] R. Spelat, F. Ferro, F. Curcio, Serine 111 phosphorylation regulates OCT4A protein subcellular distribution and degradation, J. Biol. Chem. 287 (2012) 38279–38288.
[16] P.N. Malak, B. Dannenmann, A. Hirth, O.C. Rothfuss, K. Schulze-Osthoff, Novel AKT phosphorylation sites identified in the pluripotency factors OCT4, SOX2 and KLF4, Cell Cycle 14 (2015) 3748–3754.
[17] E. Kinoshita, E. Kinoshita-Kikuta, K. Takiyama, T. Koike, Phosphate-binding tag, a new tool to visualize phosphorylated proteins, Mol. Cell. Proteomics 5 (2006) 749–757.
[18] R. Amanchy, B. Periaswamy, S. Mathivanan, R. Reddy, S.G. Tattikota, A. Pandey, A curated compendium of phosphorylation motifs, Nat. Biotechnol. 25 (2007) 285–286.
[19] Ubersax JA, Ferrell JE, Jr. Mechanisms of specificity in protein phosphorylation. Nat Rev Mol Cell Biol. 2007;8:530–41.
[20] Q.L. Ying, J. Wray, J. Nichols, L. Batlle-Morera, B. Doble, J. Woodgett, et al., The ground state of embryonic stem cell self-renewal, Nature. 453 (2008) 519–523.
[21] M. Malumbres, Cyclin-dependent kinases, Genome Biol. 15 (2014) 122.
[22] S. Larochelle, K.A. Merrick, M.E. Terret, L. Wohlbold, N.M. Barboza, C. Zhang, et al., Requirements for Cdk7 in the assembly of Cdk1/cyclin B and activation of Cdk2 revealed by chemical genetics in human cells, Mol. Cell 25 (2007) 839–850.
[23] S. Dalton, Linking the cell cycle to cell fate decisions, Trends Cell Biol. 25 (2015) 592–600.
[24] J. White, S. Dalton, Cell cycle control of embryonic stem cells, Stem Cell Rev. 1 (2005) 131–138.
[25] P.A. Chong, H. Lin, J.L. Wrana, J.D. Forman-Kay, Coupling of tandem Smad ubiquitination regulatory factor (Smurf) WW domains modulates target specificity, Proc. Natl. Acad. Sci. U. S. A. 107 (2010) 18404–18409.
[26] H.M. Xu, B. Liao, Q.J. Zhang, B.B. Wang, H. Li, X.M. Zhong, et al., Wwp2, an E3 ubiquitin ligase that targets transcription factor Oct-4 for ubiquitination, J. Biol. Chem. 279 (2004) 23495–23503.
[27] H. Yoshizaki, S. Okuda, Elucidation of the evolutionary expansion of phosphorylation signaling networks using comparative phosphomotif analysis, BMC Genomics 15 (2014) 546.

[28] E. Aragon, N. Goerner, Q. Xi, T. Gomes, S. Gao, J. Massague, et al., Structural basis for the versatile interactions of Smad7 with regulator WW domains in TGF-beta pathways, Structure. 20 (2012) 1726–1736.
[29] A.C. Mullen, D.A. Orlando, J.J. Newman, J. Loven, R.M. Kumar, S. Bilodeau, et al., Master transcription factors determine cell-type-specific responses to TGF-beta signaling, Cell. 147 (2011) 565–576.
[30] X. Chen, H. Xu, P. Yuan, F. Fang, M. Huss, V.B. Vega, et al., Integration of external signaling pathways with the core transcriptional network in embryonic stem cells, Cell. 133 (2008) 1106–1117.
[31] K.C. Davidson, E.A. Mason, M.F. Pera, The pluripotent state in mouse and human, Development. 142 (2015) 3090–3099.
[32] I. Chambers, J. Silva, D. Colby, J. Nichols, B. Nijmeijer, M. Robertson, et al., Nanog safeguards pluripotency and mediates germline development, Nature. 450 (2007) 1230–1234.
[33] S. Munoz Descalzo, P. Rue, J. Garcia-Ojalvo, A. Martinez Arias, Correlations between the levels of Oct4 and Nanog as a signature for naive pluripotency in mouse embryonic stem cells, Stem Cells 30 (2012) 2683–2691.
[34] M. Bodak, D. Cirera-Salinas, J. Yu, R.P. Ngondo, C. Ciaudo, Dicer, a new regulator of pluripotency exit and LINE-1 elements in mouse embryonic stem cells, FEBS Open Bio. 7 (2017) 204–220.
[35] D. Cirera-Salinas, C. Ciaudo, Exit from pluripotency assay of mouse embryonic stem cells, Bio-Protocol. 7 (2017).
[36] H. Niwa, J. Miyazaki, A.G. Smith, Quantitative expression of Oct-3/4 defines differentiation, dedifferentiation or self-renewal of ES cells, Nat. Genet. 24 (2000) 372–376.
[37] P.P. Tam, D.A. Loebel, Gene function in mouse embryogenesis: get set for gastrulation, Nat Rev Genet. 8 (2007) 368–381.
[38] Q.L. Ying, M. Stavridis, D. Griffiths, M. Li, A. Smith, Conversion of embryonic stem cells into neuroectodermal precursors in adherent monoculture, Nat. Biotechnol. 21 (2003) 183–186.
[39] R.P. Ngondo, D. Cirera-Salinas, J. Yu, H. Wischnewski, M. Bodak, S. Vandormael-Pournin, et al., Argonaute 2 is required for extra-embryonic endoderm differentiation of mouse embryonic stem cells, Stem Cell Reports. 10 (2018) 461–476.
[40] K.M. Loh, L.T. Ang, J. Zhang, V. Kumar, J. Ang, J.Q. Auyeong, et al., Efficient endoderm induction from human pluripotent stem cells by logically directing signals controlling lineage bifurcations, Cell Stem Cell 14 (2014) 237–252.